



Society for Science and Education  
United Kingdom

ISSN: 2055 - 1266  
Volume 5 No 5  
October, 2018

# JOURNAL OF BIOMEDICAL ENGINEERING AND MEDICAL IMAGING



---

## TABLE OF CONTENTS

EDITORIAL ADVISORY BOARD	I
DISCLAIMER	II
<b>Study of Thyroid Abnormalities using Scintigraphy</b> Amel Bushra. Ahmed <sup>1,2</sup> , Mohamed Yousef <sup>1, 3</sup> , Salah Ali Fadhlallah <sup>1</sup>	1
<b>Effect of Wall Variable Thickness on Patient Specific Finite Element Abdominal Aortic Aneurysm Models</b> Omar Altwijri	6
<b>Improvement of Sonographic Appearance Using HAT-TOP Methods</b> Yousif Mohamed Y. Abdallah	13
<b>Classification and Diagnosis of Cardiac Arrhythmia using an ECG-based Ensemble Approach</b> Ank Agarwal, Akshar Agarwal	20

# EDITORIAL ADVISORY BOARD

## Editor-in-Chief

**Prof. Kenji Suzuki**

Department of Radiology, University of Chicago  
United States

---

## Members

**Prof. Habib Zaidi**

Dept. of Radiology, Div. of Nuclear Medicine  
Geneva University Hospital, Geneva  
Switzerland

**Prof. Tzung-Pe**

National University of Kaohsiung, Taiwan  
China

**Prof. Nicoladie Tam**

Dept. of Biological Sciences, University of North Texas  
United States

**Prof. David J Yang**

The University of Texas MD Anderson Cancer Center, Houston  
United States

**Prof. Ge Wang**

Biomedical Imaging Center  
Rensselaer Polytechnic Institute Troy, New York  
United States

**Dr Hafiz M. R. Khan**

Department of Biostatistics, Florida International University  
United States

**Dr Saad Zakko**

Director of Nuclear Medicine Dubai Hospital  
UAE

**Dr Abdul Basit**

Malaysia School of Information Technology, Monash  
University  
Malaysia

**Prof. Christian L. Althaus**

University of Bern  
Switzerland

**Prof. Zandrea Ambrose**

University of Pittsburgh  
United States

**Prof. Anthony S Amend**

University of Hawaii at Manoa  
United States

**Prof. Antonio Amorim**

Universidade do Porto  
Portugal

**Prof. William Amos**

University of Cambridge  
United Kingdom

**Prof. Rachel L. Allen**

University of London  
United Kingdom

**Prof. Heike Allgayer**

University of Heidelberg  
Germany

**Prof. Virginia Abdala**

UNT-CONICET  
Argentina

**Prof. Robert B Abramovitch**

Michigan State University  
United States

**Prof. Arti Ahluwalia**

University of Pisa  
Italy

**Prof. Maria Cristina Albertini**

University of Urbino  
Italy

**Dr. Virginia Abdala**

UNT-CONICET  
Argentina

**Dr. Jafri M. Abdullah**

Fellow of the Academy of Sciences, Universiti Sains  
Malaysia

**Prof. Robert B Abramovitch**

Michigan State University  
United States

**Dr. Irina U Agoulnik**

Florida International University College of Medicine  
United States

**Prof. Arti Ahluwalia**

University of Pisa  
Italy

**Dr. Sonja-Verena Albers**

University of Freiburg  
Germany

**Prof. Maria Cristina Albertini**

University of Urbino  
Italy

**Prof. SUnited Statesn C Alberts**

Duke University  
United States

**Prof. Dawn N Albertson**

Minnesota State University, Mankato  
United States

**Dr. Silvia Alessi-Severini**

University of Manitoba  
Canada

**Dr. Veerasathpurush Allareddy**

University of Iowa  
United States

**Prof. Patrick Aloy**

Institute for Research in Biomedicine  
Spain

**Prof. Gerhard Andersson**

Linkoping University  
Sweden

**Prof. Nigel R. Andrew**

University of New England  
United Kingdom

**Prof. Martin Anger**

Central European Institute of Technology (CEITEC)  
Czech Republic

**Prof. Maria Anisimova**

Zurich University of Applied Sciences  
Switzerland

**Prof. Jérémy Anquetin**

JURASSICA Museum in Porrentruy  
Switzerland

**Prof. Praveen Arany**

University at Buffalo  
United States

**Dr. Ignacio Arganda-Carreras**

Ikerbasque, Basque Foundation for Science  
Spain

**Prof. Irina U Agoulnik**

Florida International University College of Medicine  
United States

**Prof. Sonja-Verena Albers**

University of Freiburg  
Germany

**Prof. Silvia Alessi-Severini**

University of Manitoba  
Canada

**Prof. Rachel L. Allen**  
University of London  
*United Kingdom*

**Prof. Heike Allgayer**  
University of Heidelberg  
*Germany*

**Prof. Patrick Aloy**  
Institute for Research in Biomedicine  
*Spain*

**Prof. Christian L. Althaus**  
University of Bern  
*Switzerland*

**Prof. Antonio Amorim**  
Universidade do Porto  
*Portugal*

**Prof. Gerhard Andersson**  
Linköping University  
*Sweden*

**Prof. Martin Anger**  
Central European Institute of Technology (CEITEC)  
*Czech Republic*

**Prof. Maria Anisimova**  
Zurich University of Applied Sciences  
*Switzerland*

**Prof. Louise Barrett**  
University of Lethbridge  
*Canada*

**Prof. Kerstin Bartscherer**  
Max Planck Institute for Molecular Biomedicine  
*Germany*

**Dr. Ugo Bastolla**  
Universidad Autónoma de Madrid  
*Spain*

**Prof. Amanda E Bates**  
University of Southampton  
*United Kingdom*

**Prof. Isabel Bäurle**  
University of Potsdam  
*Germany*

**Prof. Gerrit T.S. Beemster**  
University of Antwerp  
*Belgium*

**Prof. Maria del Mar Bibiloni Esteva**  
University of the Balearic Islands  
*Spain*

**Prof. Kate N Bishop**  
The Francis Crick Institute  
*United Kingdom*

**Prof. Ton Bisseling**  
Wageningen University  
*Netherlands*

**Prof. Anne Blangy**  
Montpellier University  
*France*

**Prof. Marnie E Blewitt**  
The Walter and Eliza Hall Institute of Medical Research  
*Australia*

**Prof. Anna M. Borghi**  
University of Bologna  
*Italy*

**Prof. Bettina Böttcher**  
Bayerische Julius-Maximilians-Universität Würzburg  
*Germany*

**Prof. Jürgen C Becker**  
Medical University of Graz  
*Austria*

**Prof. Laura M Boykin**  
The University of Western Australia  
*Australia*

**Prof. Ignacio Arganda-Carreras**  
Ikerbasque, Basque Foundation for Science  
*Spain*

**Prof. Nebojsa N Arsenijevic**  
University of Kragujevac  
*Serbia*

**Prof. Spyros Artavanis-Tsakonas**  
Harvard Medical School  
*United States*

**Prof. Ramy K Aziz**  
Faculty of Pharmacy, Cairo University  
*Cairo*

**Prof. Thomas Backhaus**  
University of Gothenburg  
*Sweden*

**Prof. Nicholas A Badcock**  
Macquarie University  
*Australia*

**Prof. Elena E Bagley**  
University of Sydney  
*Australia*

**Prof. Vladimir B Bajic**  
King Abdullah University of Science and Technology (KAUST)  
*Saudi Arabia*

**Dr. Stefan D Baral**  
Johns Hopkins School of Public Health  
*United States*

**Prof. Tom Bourne**  
Imperial College, London  
*United Kingdom*

**Prof. Sheila M. Bowyer**  
University of Pretoria  
*South Africa*

**Prof. Mark Boyes**  
Curtin University of Technology  
*Australia*

**Prof. Erika M Braga**  
Federal University of Minas Gerais (UFMG)  
*Brazil*

**Prof. Ebba Brakenhielm**  
Rouen University  
*France*

**Prof. Paolo Brambilla**  
University of Udine  
*Italy*

**Prof. Vincenzo Brancaleone**  
University of Naples Federico II  
*Italy*

**Prof. Björn Brembs**  
Universität Regensburg  
*Germany*

**Prof. Fiona S. Brinkman**  
Simon Fraser University  
*Canada*

**Prof. Jon Brock**  
Macquarie University  
*Australia*

**Prof. Eoin L. Brodie**  
Lawrence Berkeley National Laboratory  
*United States*

**Prof. Jacqueline Batley**  
University of Western Australia  
*Australia*

**Prof. Peter D Baade**  
Cancer Council Queensland  
*Australia*

## **DISCLAIMER**

**All the contributions are published in good faith and intentions to promote and encourage research activities around the globe. The contributions are property of their respective authors/owners and the journal is not responsible for any content that hurts someone's views or feelings etc.**



## Study of Thyroid Abnormalities using Scintigraphy

Amel Bushra. Ahmed<sup>1,2</sup>, Mohamed Yousef<sup>1,3</sup>, Salah Ali Fadhlalah<sup>1</sup>

<sup>1</sup>College of Medical Radiological Science, Sudan University of science and Technology, Sudan Khartoum

<sup>2</sup>Fujairah Hospital, Fujairah, UAE

<sup>3</sup>College of Batterjee Science College, Radiological Science, Jeddah, Saudi Arabia

Amel.Abakar@moh.gov.ae

### ABSTRACT

Radionuclide imaging is an integral part of functional evaluation of thyroid diseases. This study aimed to study thyroid abnormalities using scintigraphy, The study population consisted of 173(149 female and 24 male) patients with thyroid abnormalities, and referred to Nuclear Medicine, Fujairah hospital for thyroid scintigraphy during the period from Jan 10, 2016 to June 30, 2018. All patients Thyroid function test were done before coming to radiology department. The mean age of patients was 38 years.

The results of this study revealed that thyroid nuclear medicine scan findings as normal in 6.4 % (16 patients) and abnormal in 91% (157 patients) , Autonomous Nodule 2 (1.1),nodular goiter- NTG , TNG 30 (17.3%),Goiter11(6.4%),Grave disease13(7.5%), Multinodular goiter 43(24.8%), Thyroiditis 20 (11), Thyroid nodule 2 (1.1), Toxic multinodular goiter 21 ,Toxic goiter 15 (8.7%), Normal 16 (9.2%).

This study concluded that radionuclide methods are complementary and provide information that can help in the appropriate management of various thyroid diseases.

**Key words:** Scintigraphy, goitre, Graves' disease, thyroid nodule

### 1 Introduction

The thyroid gland is located in the neck, superior to the trachea and between the thyroid cartilage and sternal notch. The gland is relatively small, consisting of 2 lobes, each of which is approximately 2–3 cm wide by 5 cm high. <sup>[1]</sup>.

Thyroid gland has the unique ability to take up iodine — an essential component of its hormones. The phenomenon of accumulation of iodine in the thyroid gland allowed for the use of iodine isotopes in the diagnosis of thyroid disease as early as about 70 years ago, although the mechanism of iodine uptake at the molecular level has been carefully examined until the late twentieth century. In 1939, a group of scientists from the University of Berkeley documented the uptake of radioactive iodine in human thyroid for the first time. This gave rise to first therapeutic radioiodine applications in patients with hyperthyroidism and thyroid cancer <sup>[2,3]</sup>. Nowadays, we know that the uptake of iodine in the thyroid gland is attributed to the sodium-iodide symporter (NIS), described in 1993 by Kaminsky et al <sup>[4]</sup>. The uptake of iodine by the thyroid cells is still widely used in the evaluation of thyroid function by means of

radioiodine uptake test and thyroid scintigraphy [5]. This study aimed to study thyroid abnormalities using scintigraphy

## 2 Materials and methods

A total of 173 patients were seen by surgeons and medical doctors as having thyroid issues, and referred to Nuclear Medicine and Radiology Department, Fujairah hospital for thyroid scintigraphy and neck ultrasound during the period from Jan. 10, 2016 to June. 30, 2018.

The thyroid scintigraphy obtained 10-20 minutes after intravenous injection of 37-111MBq of sodium pertechnetate Tc-99m using a LEHR (low energy high resolution collimator-equipped gamma-scintillation camera. All thyroid scintigraphies were interpreted by one Nuclear Medicine Physician. For ultrasound, all patients were scanned supine with their necks hyperextended using a 7.5-10-MHz transducer. All patients underwent neck ultrasound by one expert radiologist. The data analyzed using the SPSS program.

## 3 Nuclear medicine examination

Technetium 99m pertechnetate ( $^{99m}\text{TcO}_4^-$ ) is a used radioactive label for thyroid scanning. Injection Technique a fine Butterfly needle (gauge 23-25 according to patient's age) is recommended. Technetium-99m when used as a radioactive tracer can be detected in the body by medical equipment (gamma cameras). It is well suited to the role because it emits readily detectable 140 keV gamma rays (these are about the same wavelength as emitted by conventional X-ray diagnostic equipment), and its half-life for gamma emission is 6.0058 hours (meaning 93.7% of it decays to  $^{99}\text{Tc}$  in 24 hours). The "short" physical half-life of the isotope and its biological half-life of 1 day (in terms of human activity and metabolism) allows for scanning procedures which collect data rapidly, but keep total patient radiation exposure low. The same characteristics make the isotope suitable only for diagnostic but never therapeutic use.

## 4 Data Collection and Analysis

Data will be collected in tabulated database sheet and will be analyzed by SPSS. The data included the age, gender, Us finding and Nuclear medicine scintigraphy findings

## 5 Results

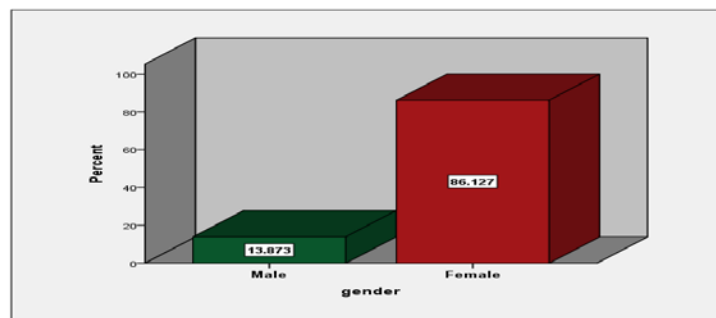


Figure 1 shows gender of the patients

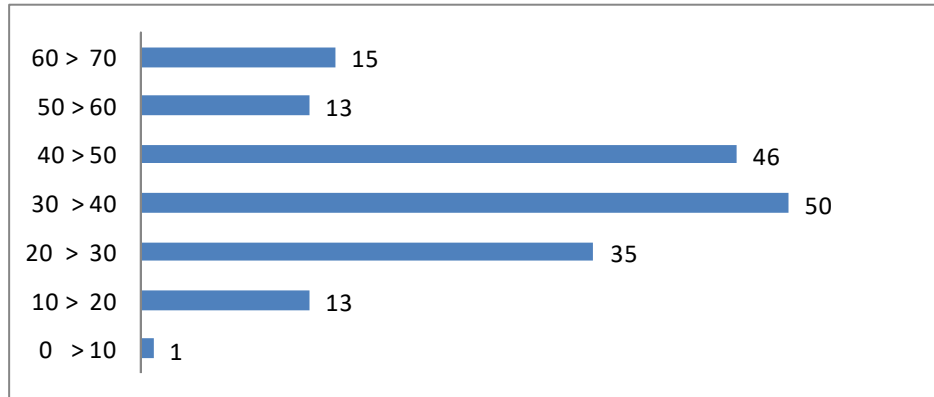


Figure 2 shows patient's ages

Table 1 shows NM findings

Thyroid disorders	Frequency
Autonomous Nodule	2 (1.1)
nodular goiter- NTG , TNG	30 (17.3%)
Goiter	11(6.4%)
Grave disease	13(7.5%)
Multinodular goiter	43(24.8%)
Thyroiditis	20 (11)
Thyroid nodule	2 (1.1)
Toxic multinodular goiter	21
Toxic goiter	15 (8.7%)
Normal	16 (9.2%)
total	173

Table 2 shows Nodules sites

Nodule site	Frequency
Lt lobe	63
Rt lobe	80
isthmus	19
Total	162

Table 3 shows Thyroid size

size	Frequency
Normal	49 (28%)
Enlarge	124 (72%)
Total	173 (100%)

## 6 Discussion

Nuclear scintigraphy is commonly used for evaluation of physiologic thyroid function and for identification of metabolically active and inactive nodules.

Nuclear medicine thyroid scan was performed by an Bright View gamma camera. Nuclear medicine classification based on distribution of the radioisotopes through the thyroid. Features were performed by one experienced nuclear medicine technologist. Size was measured as the whole diameter. The features included, homogeneity, uptake, count per pixel, and area.

The study population consisted of 173 patients were seen by surgeons and medical doctors as having thyroid issues, and referred to Nuclear Medicine and Radiology Department, Fujairah hospital for thyroid scintigraphy and neck ultrasound during the period from Jan. 10, 2016 to June. 30, 2018. All patients Thyroid function test were done before coming to radiology department. So all results were comparing with the TFT results.

nuclear medicine thyroid scintigraphy and demographic data are presented in Tables and figures for this study revealed that, among this 173 patients 86% were female (149) and 14% were male (24), fig(1). The mean age of patients was 38 years, thyroid nuclear medicine scan were reported as normal in 6.4% (16 patients) and abnormal in 91% (157 patients).

In this study table (1) shows that nuclear medicine is able to detect multi nodules in 43 patients. and if multi nodules are toxic, nuclear medicine is better in detecting it (21 patients) In diagnosis of Autonomous nodule nuclear scan was able to detect it In graves' disease nuclear medicine (13 patients) 7.5% in detecting it. For thyroiditis nuclear medicine, (25 patients) 14.4% to (20 patients) 11%. However in diagnosis of toxic goiter nuclear medicine thyroid scan was better than ultrasound, (15 patients) 8.7%

Table (2) shows the nodule sites in the Rt lobe, Lt lobe and isthmus, 80, 63, 19 in the thyroid nuclear medicine scan.

Table (3) shows that the thyroid gland size if its enlarge or not. In nuclear medicine thyroid scan it was enlarge in (124 patients) 72% of patients and normal in (49 patients) 28% of all cases.

In spite of some limitations of this, ultrasound examination plays an important role for patients in diagnosis of thyroid abnormalities, especially in thyroid nodules.

## 7 Conclusion

This study concluded that radionuclide methods can be able to provide information that can help in the appropriate management of various thyroid diseases.

## REFERENCES

- [1] Drew HH, LaFrance ND, Chen JS. Thyroid imaging studies. J Nucl Med Technol. 1987;15:79–87
- [2] Becker DV, Sawin CT. Radioiodine and thyroid disease: the beginning. Semin Nucl Med 1996; 26: 155–164.

- [3] Keston AS, Ball RP, Frantz VK, Palmer WW. Storage of radioactive iodine in a metastasis from thyroid carcinoma. *Science* 1942; 2466: 362–363.
  
- [4] Kaminsky SM, Levy O, Salvador C, Dai G, Carrasco N. The Na<sup>+</sup>/I symporter of the thyroid gland. *Soc Gen Physiol Ser* 1993; 48: 251–262.
  
- [5] Chung JK. Sodium iodide symporter: its role in nuclear medicine. *J Nucl Med* 2002; 43: 1188–1200.

# Effect of Wall Variable Thickness on Patient Specific Finite Element Abdominal Aortic Aneurysm Models

Omar Altwijri

*Biomedical Technology Department, College of Applied Medical Sciences, King Saud University, Riyadh, KSA*

[oaltwijri@ksu.edu.sa](mailto:oaltwijri@ksu.edu.sa)

## ABSTRACT

The aim of this study is to analyze the possibilities to measure the wall stress on the thinnest and thickest side of the AAA by using patient's Specific Finite Element (SFE) models, in order for understanding the rupture of AAA in a better approach. Patient specific model with different in position, Finite Element Analysis (FEA) models that were studied earlier by Di Martino et al. (1998) [1], was adopted. The AAA was modelled as a homogenous, isotropic, incompressible, linear elastic material with Young's modulus (E) and Poisson's ratio ( $\mu$ ) having value of 0.11 MPa and  $\mu = 0.45$ , respectively. The values of E and  $\mu$  was determined from uniaxial loading tests performed on specimens of AAA. In order to cast peak systolic blood pressure of a healthy patient, pressure of 145 mmHg was directed to the internal surface of the models. FEA models of AAA were analysed using ANSYS Finite Element Package 15.0 version. Values of stress was observed on the scale of von-Mises, this method helps to locate area with highest stress i.e. to calculate failure criteria by combining the stress in three-dimensions. In order to determine the collapse of AAA wall von-Mises stress is commonly use for the assessment of the AAA stress. Our findings and results strengthens the earlier studies performed by Polzer et al. (2010) [2] and Altuwajiri (2015) [3], where AAA wall stress was reduced by formation of thrombus. Thus reducing the chance of AAA rupture and supporting the wall strength. Our findings suggest that thrombus clearly works as a shield to guard the AAA wall from rupture. However, more research and further studies are required that corroborate the relation between the biological and mechanical factors to understand the role of the thrombus for AAA rupture.

**Keywords:** Abdominal aortic aneurysm, Wall thickness.

## 1 Introduction

Pathological dilatations of aneurysm are irreversible and enduring, that can occur in any blood vessel [4]. Aneurysm dilatations are of serious concern, when occur at the infrarenal section of the abdominal aorta. Abdominal Aorta Aneurysm (AAA) [4], can eventually rupture if left untreated, with a mortality rate of 90% among ruptured patients [5]. Claiming around 15,000 lives annually in America [6]. AAA's are considered to be proactive when the abdominal aorta reaches upto 3 cm in diameter [6, 7]. Commonly, ultrasound imaging or computed tomography scans are utilize for monitoring the growth

rate of the diameter of abdominal aorta, in case the growth rate observed 1cm per year or greater, when a AAA reaches 5.5 cm, a reparative surgery is performed [7]. It has been noted that smaller AAAs with 5.5 cm can also get rupture, in contrast to larger AAAs are also found to be steady and may get pointless surgery [5, 8-11]. Thus raising a concern to perform surgery on AAAs with 5.5 cm in diameter and a growth rate of 1 cm in diameter. Therefore, further studies are required to analyse the risks of expansion and rupture for AAAs [12].

Various studies have been performed noninvasively [13] and invasively [14-16] to understand the wall strength of the AAA. These experimental studies carried out to numerically comprehend the procedure for rupture of AAA [4]. As till date limited studies executed for establishing the rupture potential. As the stress of blood pressure rises on the walls of AAA, rupture caused due to weaken in strength of the wall [17]. Truijers et al. (2007) [18] and Fillinger et al. (2002) [19], studies illustrates wall stress analyses AAA from patient-specific size on a computer-based method, using Finite element method (FEM). The geometrical dimension of the AAA is ascertain from Computed Topographic Angiography [17]. Significant difference been observed in material parameters among healthy abdominal aortas and AAA wall. According to Vorp (2007) [8], a maximum error of less than 5% can occur if standard values for these parameters are used. With the use Ultrasound technology, measurements can be measured for superficial arteries, by using a high frequency ultrasound waves. A study performed by Haller et al. (2007) [20], for analysing carotid artery by using high frequency results in high resolution images gives exceptional possibilities.

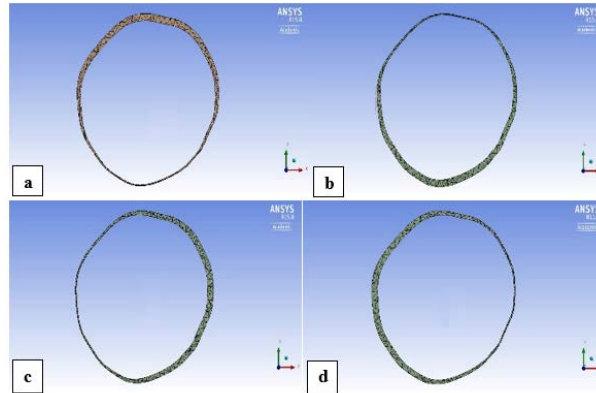
Studies on the wall stress of AAA models by using patient SFE models are complex and scarce subject. The aim of this study is to analyze the possibilities to measure the wall stress on the thinnest and thickest side of the AAA by using patient's SFE models, in order for understanding the rupture of AAA in a better approach. To the knowledge of the author, this is the very first study to analyze wall stress at the thinnest and thickest sides of the AAA.

## 2 Methodology

To simplify the AAA and model it on a CAD software. Patient specific model with different in position (Case 1, Case 2, Case 3 and Case 4) FEA models that studied earlier by Di Martino et al. (1998) [1], was adopted. A precise design and approach of AAA was used to model the CAD with the help of FEA for this study. Di Martino et al. (1998) [1], obtained the specimen's dimension and size during AAA surgery. The AAA was modelled as a homogenous, isotropic, incompressible, linear elastic material with Young's modulus (E) and Poisson's ratio ( $\mu$ ) having value of 0.11 MPa and  $\mu = 0.45$ , respectively. The values of E and  $\mu$  was determined from uniaxial loading tests performed on specimens of AAA. In order to cast peak systolic blood pressure of a healthy patient, pressure of 145 mmHg was directed to the internal surface of the models.

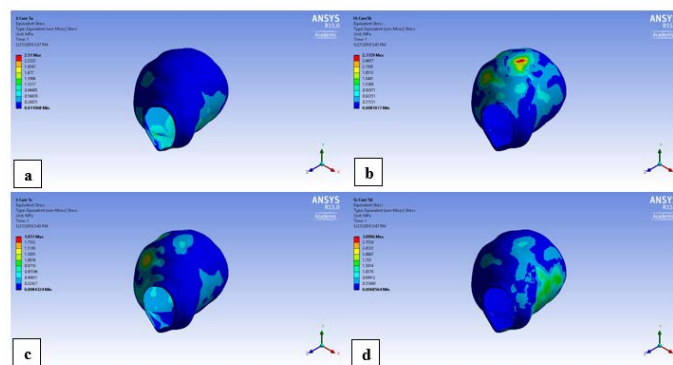
The four patient specific FEA models were sketched, extruded and analyzed using the ANSYS Finite Element Package 15.0 version (ANSYS Inc., Canonsburg, Pennsylvania, United States, and License Server 1055@PC13) at the department of Biomedical Technology, College of Applied Medical Sciences, King Saud University. The four different models are seen in Figure 1, only the thrombus thickness from inside the aneurysm varied in each model in contrast to the dimension of the models.

Case 1 AAA thickness of the lumen of blood is at anterior position as seen in Figure 1a. In figure 1b, Case 2 AAA thickness of the lumen of blood is at posterior position. Case 3 AAA thickness of the lumen of blood is at right position see figure 1c. Figure 1d, Case 4 thickness of the lumen of the AAA can be seen at the left.



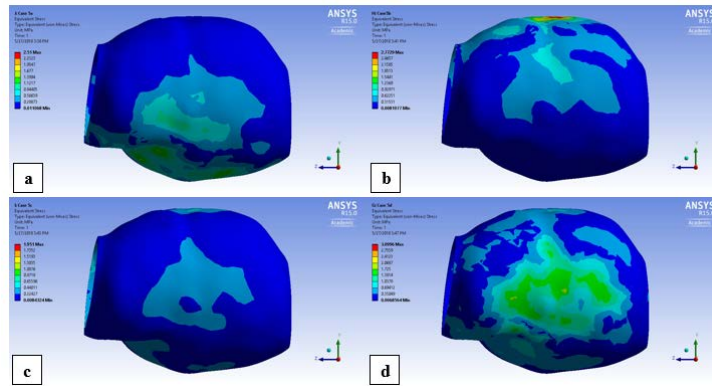
**Figure 1 Models of AAA with same thickness and thinness at different positions.**

Four FEA models of AAA were analysed using ANSYS Finite Element Package 15.0 version. Values of stress was observed on the scale of von-Mises, this method helps to locate area with highest stress i.e. to calculate failure criteria by combining the stress in three-dimensions. In order to determine the collapse of AAA wall von-Mises stress is commonly use for the assessment of the AAA stress.



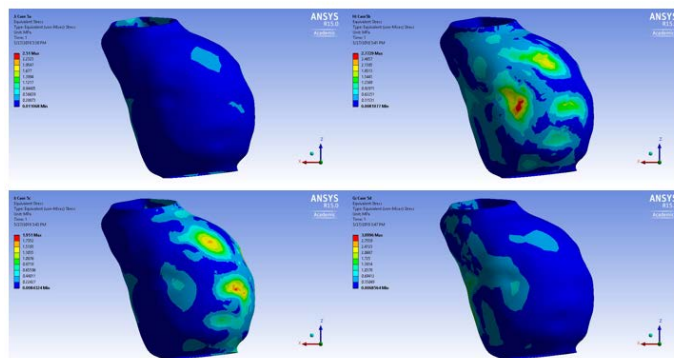
**Figure 2 Effective wall stress distribution of four models at Z and X planes**

Figure 2, displays us the four different models of AAA where von-Mises stress distribution across the walls are viewed across Z and X planes, over peak systolic pressure at static simulation. The maximum stress location is clearly visible in second model in figure 2 b, with maximum stress value of 2.7729 MPa equivalent to (von-Mises) stress, as AAA rupture is obvious to happen at the thinnest side of the wall.



**Figure 3** Effective wall stress distribution of four models at X plane

In figure 3 we can see four different models of AAA where von-Mises stress distribution across the walls are viewed across X plane, over peak systolic pressure at static simulation. The maximum stress location is again visible in second model (figure 3 b) with maximum stress value of 2.7729 MPa equivalent to (von-Mises) stress, as AAA rupture is obvious to happen at the thinnest side of the wall.



**Figure 4** Effective wall stress distribution of four models at Y plane

Four different models of AAA where von-Mises stress distribution across the walls are viewed across Y plane can be seen in figure 4, where peak systolic pressure at static simulation. The maximum stress location is visible in second and third models with maximum stress value of 2.7729 MPa and 1.951 MPa, respectively, equivalent to (von-Mises) stress, as AAA rupture is obvious to happen at the thinnest side of the wall.

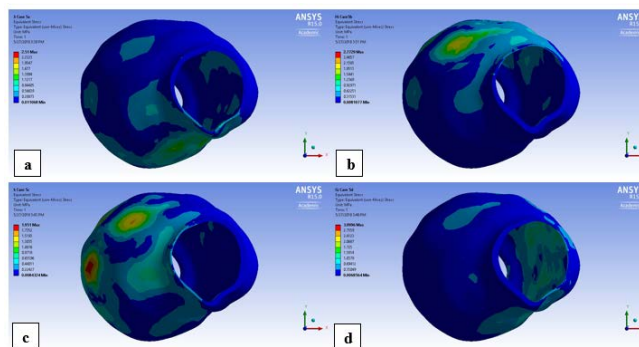


**Figure 5** Effective wall stress distribution of four models at X plane

As seen in figure 5, four different models of AAA where von-Mises stress distribution across the walls are viewed across Z plane, where peak systolic pressure at static simulation. The maximum stress location is only visible in third model (can be seen in figure 5 c) with a maximum stress value of 1.951 MPa equivalent to (von-Mises) stress, as AAA rupture is obvious to happen at the thinnest side of the wall.

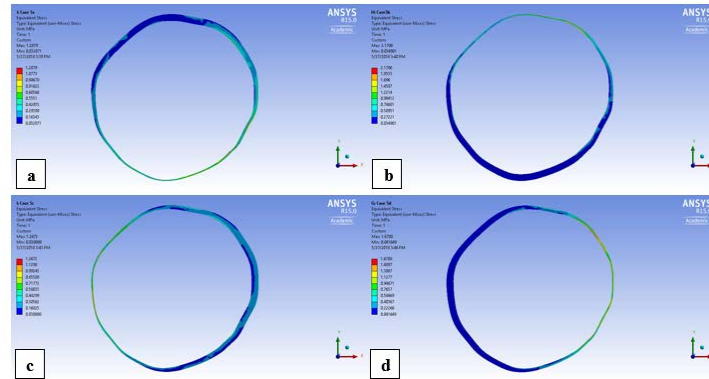


**Figure 6 Effect of variable wall thickness on wall stress distribution of four models**

The minimum and maximum stress at the thinnest side after slicing and meshing from the center of all the four models of AAA were found to be similar. In the first and second models, the thinnest side (at bottom for first model, see figure 6A and top for second model, see figure 6B) exhibits a minimum stress level 0.40 MPa and maximum stress level of 2.5 equivalent stress. Similarly, for the third and fourth models the thinnest side (at left for third model, see figure 5C and right for fourth model, see figure 5D) exhibits a minimum stress level 0.48 MPa and maximum stress level of 2.5 equivalent stress.

### 3 Discussion

The aim of this study was to analyse the rupture among different models of AAA and compare their stress values at thin and thick sides of the models. Till date there has been no study with in-vitro rupture of AAA's with different position models constructed with the help of CAD software. In addition, many studies are earlier performed with computational analysis to understand the rupture of AAAs [9, 21-23]. Although all four models were designed using the ANSYS FEA technique there have been a different stress values recorded at the thinnest side. First two models with AAA thickness at anterior and posterior bears equal and higher amount of stress, while the thinnest side where rupture is most likely to occur have equal and less amount of stress. Moreover, when the thickness of AAA is at right and left display equal and higher amount of stress similar to earlier two models. However, the thinnest side exhibits an equal amount of stress but in contrast a higher stress values when compared with the first two models. Our findings and results strengthens the earlier studies performed by Polzer et al. (2010) [2] and Altuwajri (2015) [3], where AAA wall stress was reduced by formation of thrombus. Thus reducing the chance of AAA rupture and supporting the wall strength. However, a clinical study by Schurink et al. (2000) [24], contradicts our findings where formation of thrombus increases the chance of AAA rupture.

Our findings suggest that thrombus clearly works as a shield to guard the AAA wall from rupture. However, more research and further studies are required that corroborate the relation between the biological and mechanical factors to understand the role of the thrombus for AAA rupture.

## ACKNOWLEDGEMENT

The authors extend their appreciation to the Deanship of Scientific Research at King Saud University for funding this work through the Research Project No NFG-14-02-16.

## REFERENCES

- [1] Di Martino, E.S., et al., Fluid–structure interaction within realistic three-dimensional models of the aneurysmatic aorta as a guidance to assess the risk of rupture of the aneurysm. *Medical engineering & physics*, 2001. 23(9): p. 647-655.
- [2] Polzer, S. and J. Bursa. Poroelastic model of intraluminal thrombus in FEA of aortic aneurysm. in 6th World Congress of Biomechanics (WCB 2010). August 1-6, 2010 Singapore. 2010. Springer.
- [3] Altuwijri, O. Finite Element Analysis OF Abdominal Aortic Aneurysms to Predict Risk of Rupture- The Role of The Thrombosis Thicknesses. in World Congress on Medical Physics and Biomedical Engineering, June 7-12, 2015, Toronto, Canada. 2015. Springer.
- [4] Doyle, B.J., et al., An experimental and numerical comparison of the rupture locations of an abdominal aortic aneurysm. *Journal of Endovascular Therapy*, 2009. 16(3): p. 322-335.
- [5] Vorp, D.A. and J.P.V. Geest, Biomechanical determinants of abdominal aortic aneurysm rupture. *Arteriosclerosis, thrombosis, and vascular biology*, 2005. 25(8): p. 1558-1566.
- [6] McGloughlin, T.M. and B.J. Doyle, New approaches to abdominal aortic aneurysm rupture risk assessment: engineering insights with clinical gain. *Arteriosclerosis, thrombosis, and vascular biology*, 2010. 30(9): p. 1687-1694.
- [7] Martufi, G., et al., Three-dimensional geometrical characterization of abdominal aortic aneurysms: image-based wall thickness distribution. *Journal of biomechanical engineering*, 2009. 131(6): p. 061015.
- [8] Vorp, D.A., Biomechanics of abdominal aortic aneurysm. *Journal of biomechanics*, 2007. 40(9): p. 1887-1902.
- [9] Fillinger, M.F., et al., Prediction of rupture risk in abdominal aortic aneurysm during observation: wall stress versus diameter. *Journal of vascular surgery*, 2003. 37(4): p. 724-732.
- [10] Darling, R.C., et al., Autopsy study of unoperated abdominal aortic aneurysms. The case for early resection. *Circulation*, 1977. 56(3 Suppl): p. II161-4.
- [11] Nicholls, S.C., et al., Rupture in small abdominal aortic aneurysms. *Journal of vascular surgery*, 1998. 28(5): p. 884-888.
- [12] Thubrikar, M.J., J. Al-Soudi, and F. Robicsek, Wall stress studies of abdominal aortic aneurysm in a clinical model. *Annals of vascular surgery*, 2001. 15(3): p. 355-366.

- [13] Geest, J.P.V., et al., Towards a noninvasive method for determination of patient-specific wall strength distribution in abdominal aortic aneurysms. *Annals of biomedical engineering*, 2006. 34(7): p. 1098-1106.
- [14] Raghavan, M.L., et al., Regional distribution of wall thickness and failure properties of human abdominal aortic aneurysm. *Journal of biomechanics*, 2006. 39(16): p. 3010-3016.
- [15] J. Thubrikar, M.L., F. Robicsek, J. Al-Soudi, B. Fowler, M, Mechanical properties of abdominal aortic aneurysm wall. *Journal of medical engineering & technology*, 2001. 25(4): p. 133-142.
- [16] Raghavan, M.L., M.W. Webster, and D.A. Vorp, Ex vivo biomechanical behavior of abdominal aortic aneurysm: assessment using a new mathematical model. *Annals of biomedical engineering*, 1996. 24(5): p. 573-582.
- [17] Van den Hengel, W.K. and F. van de Vosse, Abdominal aortic wall thickness and compliance. 2008.
- [18] Truijers, M., et al., Wall stress analysis in small asymptomatic, symptomatic and ruptured abdominal aortic aneurysms. *European Journal of Vascular and Endovascular Surgery*, 2007. 33(4): p. 401-407.
- [19] Fillinger, M.F., et al., In vivo analysis of mechanical wall stress and abdominal aortic aneurysm rupture risk. *Journal of vascular surgery*, 2002. 36(3): p. 589-597.
- [20] Haller, C., et al., Sequential based analysis of Intima-Media Thickness (IMT) in common carotid artery studies. *Atherosclerosis*, 2007. 195(2): p. e203-e209.
- [21] McGloughlin, T.M., et al., A finite element analysis rupture index (FEARI) as an additional tool for abdominal aortic aneurysm rupture prediction. 2009.
- [22] Doyle, B.J., A. Callanan, and T.M. McGloughlin, A comparison of modelling techniques for computing wall stress in abdominal aortic aneurysms. *Biomedical engineering online*, 2007. 6(1): p. 38.
- [23] Doyle, B.J., et al., Vessel asymmetry as an additional diagnostic tool in the assessment of abdominal aortic aneurysms. *Journal of vascular surgery*, 2009. 49(2): p. 443-454.
- [24] Schurink, G., et al., Thrombus within an aortic aneurysm does not reduce pressure on the aneurysmal wall. *Journal of Vascular Surgery*, 2000. 31(3): p. 501-506.

# Improvement of Sonographic Appearance Using HAT-TOP Methods

Yousif Mohamed Y. Abdallah

*Department of Radiological Science and Medical Imaging, Faculty of Applied Medical Science, Majmaah  
University, Majmaah, Saudi Arabia;*  
[y.yousif@mu.edu.sa](mailto:y.yousif@mu.edu.sa)

## ABSTRACT

Ultrasound consider of one of the most important tool in analysis of fetus development. In ultrasound images, the recognition closely adjacent tissues is very crucial process because of the noise that affected both image quality and sharpness. This study conducted to study the fetus images improvement using HAT-TOP transform as computing choice in order to increase the diagnostic accuracy in diagnosis of neonatal diseases. Many image-processing techniques were used to improve the images including Using HAT-TOP and Blind Deconvolution Algorithm. The results of the study showed HAT-TOP was best processing filter and define the fetus precisely.

**Keywords:** Ultrasound, image processing, MatLab, HAT-TOP technique.

## 1 Introduction

Ultrasound images in general are complex due to data composition, which can be described in terms of speckle information. Upon visual inspection, speckle noise consists of a relatively high grey level intensity, qualitatively ranging between hyperechoic (bright) and hypoechoic (dark) domains. In addition, ultrasound images have the advantage of being non-invasive, portable, versatile, and low cost and not requiring ionizing radiations [1-2]. The filter preserves monotonic image features that fill more than half the area of the transform window. Based on Median filter have used Topological Median filter to improve conventional Median filter [3-4]. The Topological Median filters defined are outperforming conventional Median filters with 7 x 7 or larger transform windows in reducing a noise while preserving edges. On the average, there is a minimal effect on edge strength or edge location. A conventional Median filter does outperform a Topological Median filter in the reduction of the amplitude of noise [5]. Through experiments, the variance of noise passed through a Topological Median filter was found to exceed that of a conventional Median filter by a factor of about 1.25 [6]. The best techniques for processing such images are edge magnitude and edge location. Conventional Median filters reduce the variance of noise more than Topological Median filters. An adaptive two-pass Median filter to remove impulsive noise. An image contaminated by impulsive noise is represented in a two-pass Median filtering and is processed by a Median filter twice. By analyzing the spatial distribution, i.e., the error index matrix of the impulsive noise, the adaptive two-pass Median filter looks for columns containing over-corrected pixels by the standard Median filter and replaces over-corrected pixels by their original values[7-9]. The experiment that has been done shows that the adaptive filter is able to reduce the

---

DOI: 10.14738/jbemi.55.5283

Publication Date: 18<sup>th</sup> October 2018

URL: <http://dx.doi.org/10.14738/jbemi.55.5283>

mean square (MSE) and mean absolute error (MAE) produced better results. The image is divided into different regions using neighborhood contrast intensity and employ different methods to denoise the pixels in different regions. This is not only to maintain the characteristic that the Average filter algorithm has a better denoising effect on Gaussian noise, but take into account that Median filter algorithm can better preserve the details [10]. Experiments that been done show that the proposed algorithm is practicable and competent. Wiener filters are extensively used for inverse problems. Based on Wiener filter method considered as the adaptive Wiener filtering of noisy images and image sequences. An adaptive weighted averaging approach was used to estimate the second-order statistics required by the Wiener filter. From the experiment, it shows that the result from Wiener filter has improved the peak-to-peak signal noise ratio (PSNR) by about 1dB. It has also improved the annoying boundary noise significantly [11-12]. Image segmentation is a process to partition an image into Non-overlap regions, which is an important step in the image processing area and is fundamental to the analysis and identification in image processing. Image segmentation is an important process for most of the medical image analysis tasks, which is basic for higher-level image comprehension and analysis [13]. A good segmentation will benefit clinicians and patients as it provides important information for surgical planning, early disease detection and 3D visualization .In order to solve the problems of medical image segmentation, many practical methods have been advanced in this field. These include watershed segmentation, shareholding method, region-growing method, fuzzy cluster method and so on. The watershed algorithm is a classical and an effective segmentation method by which one-pixel wide continuous edge can be extracted [14]. The most effective methods in complex segmentation problems are watershed segmentation. The segmented region is obtained when the algorithm uses watershed transform applied to the image. However, segmentation of noisy ultrasound image using watershed transform always leads to over-segmentation [15-16]. There are many applications whether on synthesis of the objects or computer graphic images require precise segmentation. In general, image noise should be eliminated through image pre-processing [17].

## 2 Materials and Methods

This study carried out to enhance the quality of ultrasound images of long bone fracture through removal of speckle noise using techniques such as Median, Average and Wiener Filtering. The median filter is a non-linear digital filtering technique; it used to remove noise from images. It is useful to reduce speckle noise and salt and pepper noise. Its edge-preserving nature makes it practical in cases where edge blurring is undesirable. Average Filter performs spatial filtering on each individual pixel in an image using the grey level values in a square or rectangular window surrounding each pixel.

### Image analysis using MatLab:

#### Top-hat filtering.

The morphological algorithm accomplishes on the grayscale sonographs. It uses opening technique then subtracts the product from the inventive image.  $imtophat$  uses the structuring element SE, where SE is returned by  $strel$ . SE use to computing single structure rather than multiple.  $IM2 = imtophat(IM, NHOOD)$  where NHOOD is an array of 0s and 1s that specifies the size and shape of the structuring element, is the same as  $imptophat(IM, strel(NHOOD))$ . The steps of processing is shown in figure 1.

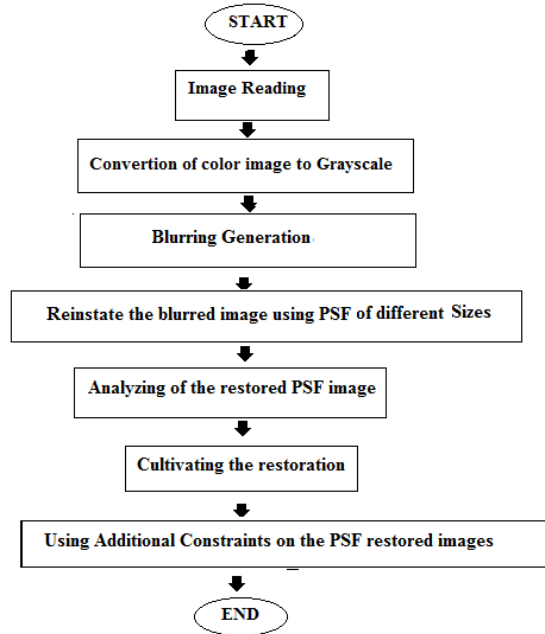


Figure 1. Top-hat filtering processing steps

The data analyzed by using MatLab program to enhance the contrast within the soft tissues, the gray levels in both enhanced and unenhanced images and noise variance.

### 3 Results

Ultrasound images in general are complex due to data composition, which can be described in terms of speckle information. Upon visual inspection, speckle noise consists of a relatively high grey level intensity, qualitatively ranging between hyperechoic (bright) and hypoechoic (dark) domains. In addition, ultrasound images have the advantage of being non-invasive, portable, versatile, and low cost and not requiring ionizing radiations. Therefore, those images need to be modified by using image processing program to get rid the noise, blurring and unwanted information.

#### Top-hat filtering

It performed morphological top-hat filtering on the grayscale or binary input image IM fig.1 and fig.2.

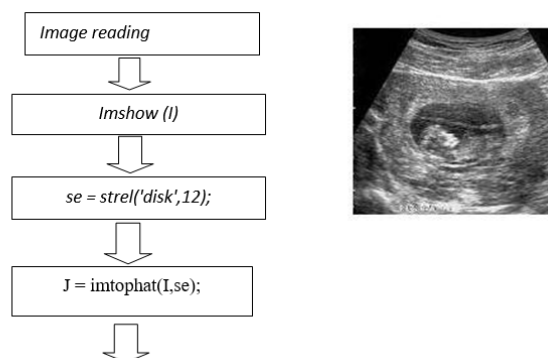


Figure 2. The Original U/S image

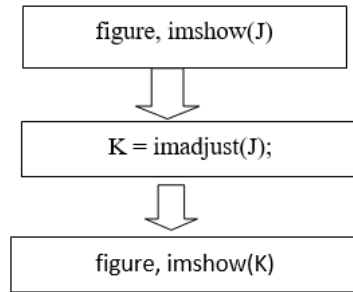


Figure 3. Top-hatted ultrasound image

## Deblurring Images Using the Blind Deconvolution Algorithm

The Blind Deconvolution Algorithm:

### Step 1: Read Image

The example reads in an intensity image. The deconvblind function can handle arrays of any dimension figure 4.



Figure 4.Original U/S image

### Step 2: Simulate a Blur



Figure 5. Shows blurred U/S image

### Step 3: Restore the Blurred Image Using PSFs of Various Sizes



Figure 7. Shows Deblurring with Oversized PSF for U/S image



Figure 6. Shows blurred U/S image



Figure 8. Shows Deblurring with INITPSF for U/S image

### Step 4: Evaluating the Restored PSF

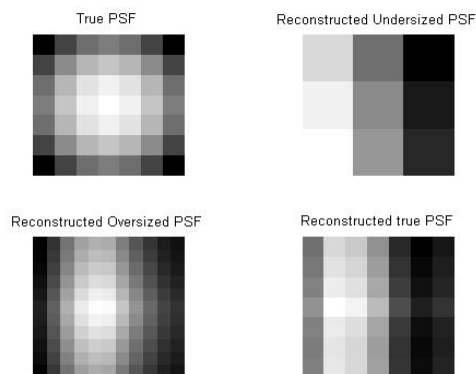


Figure 9. Shows Analyzing the Restored PSF for U/S image

## Step 5: Improving the Restoration



Figure 10. Shows Improving the Restoration of U/S image

## Step 6: Using Additional Constraints on the PSF Restoration



Figure 11. Shows Deblurred Image



Figure 12. Shows anonymous function Deblurred Image

## 4 Conclusion

Ultrasound images in general are complex due to data composition, which can be described in terms of speckle information. Upon visual inspection, speckle noise consists of a relatively high grey level intensity, qualitatively ranging between hyperechoic (bright) and hypoechoic (dark) domains. In addition, ultrasound images have the advantage of being non-invasive, portable, versatile, and low cost and not requiring ionizing radiations. Therefore, those images need to be modified by using image processing program to get rid the noise, blurring and unwanted information. This was an experimental study to study the enhancement of ultrasound image using filtering technique using image-processing technique. In addition, to evaluate contrast enhancement pattern in different ultrasound images such as grey color in order to evaluate the usage of new nonlinear approach for contrast enhancement of soft tissues in panoramic images. The main techniques of enhancement used in this study was Top-hat filtering and Blind Deconvolution Algorithm The results of this study were agreed with previous studies in blind Deconvolution algorithm and it added new approach by using both technique in U/S image processing which would increase the diagnostic value of those images. So conclusion of this research that the new method is supported that the best method to solve BSS presence by filtering the noise and background. The detection of the noise is a complex procedure, which is difficult to detect by naked eye so that image analysis should be performed by using powerful image processing.

## REFERENCES

- [1] Abdallah, Y., Hayder, A., and Wagiallah ,E., Automatic Enhancement of Mammogram using Contrast Algorithm. International Journal of Science and Research (IJSR), 2014. 3(9): p. 1886-1891.
- [2] Abdelwahab, R., and Abdallah, Y., Hayder, A., and Wagiallah ,E., Application of Texture Analysis Algorithm for Data Extraction in Dental X-Ray Images. International Journal of Science and Research (IJSR), 2014. 3(10): p. 1934-1939.
- [3] Abdallah, Y., Alkhir, M., Algaddal, A., Improvement of Brain Tumors Detection Using Markers and Boundaries Transform. International Journal of Science and Research (IJSR), 2015. 4(1): p. 2372-2378.
- [4] Bidgood, D. & Horii, S., Introduction to the ACR-NEMA DICOM standard. RadioGraphics, 1992. 12: p. 345-355.
- [5] Lehmann, T.M.; Gönner, C. & Spitzer, K., Survey: Interpolation Methods in Medical Image Processing. IEEE Transactions on Medical Imagin: 1999. 18(11): p. 1049-1075
- [6] Li, G. & Miller, R.W., Volumetric Image Registration of Multi-modality Images of CT, MRI and PET, Biomedical Imaging. Youxin Mao (Ed.), 2010.
- [7] Abdallah, Y., Application of Analysis Approach in Noise Estimation, Using Image Processing Program. Lambert Publishing Press GmbH & Co. KG, Germany, 2011.
- [8] Lyra, M.; Sotiropoulos, M., Lagopati, N. & Gavrilleli, M. , Quantification of Myocardial Perfusion in 3D SPECT images – Stress/Rest volume differences, Imaging Systems and Techniques (IST), IEEE International Conference 2010: p. 31 – 35
- [9] Narasimha-Iyer, H., et al., Automatic Identification of Retinal Arteries and Veins From Dual-Wavelength Images Using Structural and Functional Features. Biomedical Engineering, IEEE Transactions, 2007. 54(8): p. 1427-1435.
- [10] Abdallah, Y., and Wagiallah, E., Segmentation of Thyroid Scintigraphy Using Edge Detection and Morphology Filters. International Journal of Science and Research (IJSR), 2014. 3(11): p. 2768-2772.
- [11] Abdallah, Y., and Hassan, A., Segmentation of Brain in MRI Images Using Watershed-based Technique. International Journal of Science and Research (IJSR), 2015. 4(1): p. 683-688.
- [12] Abdallah, Y., Application of Analysis Approach in Noise Estimation, Using Image Processing Program. Lambert Publishing Press GmbH & Co. KG. 2011. 123-125
- [13] Pinz, A., et al., Mapping the human retina. Medical Imaging, IEEE Transactions on, 1998. 17(4): p. 606-619.
- [14] Abdallah, Y., and Yousef R., Augmentation of X-Rays Images using Pixel Intensity Values Adjustments. International Journal of Science and Research (IJSR), 2015. 4(2): p. 2425-2430.

# Classification and Diagnosis of Cardiac Arrhythmia using an ECG-based Ensemble Approach

<sup>1</sup>Ank Agarwal, <sup>2</sup>Akshar Agarwal

<sup>1</sup>*Institute for Cell Engineering, Johns Hopkins University School of Medicine, Baltimore, Maryland, United States of America;*

<sup>2</sup>*Neurology, Yale University School of Medicine, New Haven, Connecticut, United States of America;*  
aagarw26@jhu.edu; akshar.agarwal@yale.edu

## ABSTRACT

Cardiovascular Disease (CVD) remains the leading cause of death, worldwide and in the United States. Approximately 30% of global deaths can be attributed to one form of CVD, including conditions such as heart disease, stroke, heart attack, and arrhythmia. In diagnosing CVD, electrocardiograms (ECG) are commonly used to measure and record the electrical activity of the heart. Their non-invasive, informative, and relatively simple nature allows for rapid deployment. However, because analysis of ECGs depends solely on a physician, ECG analysis becomes subjective, adding a potential layer of error to patient healthcare. Studies indicate that physicians often misread ECGs and disagree with each other's interpretations. In order to develop an accurate and objective method for ECG analysis, this study evaluates various ensemble algorithms to design and create a supervised classification model. Several ensemble models were evaluated to derive one which correctly classifies CVD with sufficiently high accuracy. A boosted decision tree ensemble created to evaluate cardiac condition performs best, with an overall accuracy of 84.6% and an AUC of 0.828.

**Keywords:** computer-aided diagnosis, arrhythmia, AI-based clinical decision making

## 1 Introduction

Cardiovascular disease (CVD) is the number one cause of death both globally and in the United States, accounting for 17.3 million deaths per year (30% of all deaths). In fact, it is estimated that the number will rise to 23.6 million deaths per year by 2030 [1].

In order to diagnose CVD, physicians utilize electrocardiogram (ECG) recordings. ECGs provide measurements, indicating the electrical activity of the heart. Despite CVD being the most prevalent cause of death worldwide, it is diagnosed using physician-based analysis of ECG data, which can potentially add subjective interpretation of patient data. In the United States, most ECGs are read by non-cardiologists with nominal training in ECG readings [2]. Furthermore, non-cardiologists often disagree on ECG analyses [3]. In the emergency room, errors in ECG analysis can delay appropriate treatment of patients at hand, as well as result in delayed treatment of patients waiting in the queue [4]. Thus, there is a clear and present need for an objective, accurate, and rapid method of ECG analysis.

Several attempts have been made in the past to produce a capable classification model for arrhythmia. Some of these studies focused on individual classifiers, such as relevance vector machines (RVM) [5]. Other approaches have attempted to utilize artificial neural networks (ANN), Markov chains, and support vector machines (SVM). Machine learning models have been applied to arrhythmia classification in the past, however the novel approach described herein utilizes an ensemble model. This ensemble approach offers a more robust model with reduced error. Therefore, multiple ensemble approaches were evaluated to accurately predict heart condition from electrocardiogram data.

## 2 Methods

### 2.1 Dataset

The dataset used herein was obtained from the University of California (UCI), Irvine Machine Learning Repository, contributed by Guvenir et al. [6,7]. The dataset contains information from 452 patients, consisting of 279 attributes. The patients' conditions are labeled as one of 16 conditions, 15 irregular and one healthy. The features primarily consist of ECG data: heart rate, PQRST wave signals, channel information, et cetera. Other features are general subject information: age, sex, height, weight, et cetera. Table 1 below shows the categories/conditions and their respective sizes from the initial study. The data was largely intact, but several datum points were missing. The 14th feature, which consisted of J point data, was missing for the overwhelming majority of patients; of the 452 patients, 376 patients had missing values for feature 14. Data from feature 14 was therefore excluded from all patients. Additionally, 32 patients had missing values in a variety of features. Therefore, instead of interpolating those data, the 32 subjects were removed altogether. Instances which were labelled as 16, miscellaneous heart conditions, were also removed. The dataset used for the machine-learning model described herein consists of 402 patients with 278 features/attributes, belonging to 11 classes. Two-class performance (healthy or ill) was also assessed for each model.

**Table 1: Instances of arrhythmia and their respective counts in the original dataset**

Condition Code	Condition	Number of instances
1	Healthy	245
2	Ischemic changes (Coronary Artery Disease)	44
3	Old Anterior Myocardial Infarction	15
4	Old Inferior Myocardial Infarction	15
5	Sinus tachycardia	13
6	Sinus bradycardia	25
7	Ventricular Premature Contraction (PVC)	3
8	Supraventricular Premature Contraction	2
9	Left bundle branch block	9
10	Right bundle branch block	50

11	1st degree AtrioVentricular (AV) block	0
12	2nd degree AV block	0
13	3rd degree AV block	0
14	Left ventricular hypertrophy	4
15	Atrial Fibrillation or Flutter	5
16	Others	22

## 2.2 Machine Learning Model

Decision trees are a standard supervised learning method and are often used for both classification and regression. Classification and Regression Trees (CART) are relatively simple and easy to implement, but come with many tradeoffs. CART models introduce high variance and are quite unstable individually. To reduce the variance that a single unstable CART model might incur, various ensembles are proposed here. Several forms of boosting and aggregation are evaluated.

Boosting is an additional method of combining individual classifiers through the specification of a cost function and majority voting. It is also well suited for decision trees. RUSBoost, a popular boosting algorithm, rectifies class imbalances by drawing a subset of samples from each class and then follows traditional reweighting procedures for creating an ensemble [8-11].

## 2.3 Implementation

Using the MATLAB Statistics and Machine Learning Toolbox, the ensemble approach was used here as it is favorable to individual CART models due to reductions in variance and overall increases in accuracy. In order to evaluate various ensembles and perform model selection, Bayesian optimization was used as described by Snoek, J et al. [12]. Bayesian optimization explores various hyperparameters in search of minimizing the objective function. This method of model and hyperparameter selection is favorable because grid searches are computationally intensive, and although random searches have been demonstrated to reduce error when certain criteria are met, Bayesian optimization produces non-trivial values in short time. A large quantity of tunable parameters exist, including, but not limited to: methods of boosting/bagging, maximum depth, minimum number of splits, split criterion, et cetera. As the number of tunable parameters increases, the time required for a grid search exponentially increases, leaving Bayesian optimization to be the preferred method. Bayesian optimization entails training a Gaussian process and computing the expected improvement. A model is constructed through exploration of certain values and predictions are made regarding which values will return the greatest expected improvement.

## 3 Results

Various ensembles were evaluated, as shown in Table 2.

**Table 2: Performance Statistics for all evaluated ensemble algorithms**

11-Class						
Data	Overall Accuracy	C-Statistic (AUC)	Sensitivity	Specificity	Predictive Value	
					Positive	Negative
Random Forest	0.8202	0.8449	0.7576	0.9241	0.8741	0.8456
RUS Boosted	0.2363	0.5524	0.3714	0.7706	0.3421	0.7925
Subspace Discriminant	0.5970	0.8059	0.8333	0.9033	0.4902	0.9798
Subspace KNN	0.5597	0.6563	0.8333	0.7771	0.1765	0.9879
2-Class						
Data	Overall Accuracy	C-Statistic (AUC)	Sensitivity	Specificity	Predictive Value	
					Positive	Negative
Random Forest	0.8458	0.8278	0.7273	0.9283	0.8759	0.8302
RUS Boosted	0.8259	0.8841	0.7975	0.9707	0.9489	0.8755
Subspace Discriminant	0.7736	0.7454	0.7833	0.8475	0.6861	0.9019
Subspace KNN	0.7139	0.6718	0.7553	0.7857	0.5182	0.9132

Bayesian optimization was iteratively performed 30 times per classifier and the configurations with the highest accuracies were evaluated. The highest 11-Class accuracy was achieved with a random forest, an extension of bootstrap aggregation [13]. Random forests have been applied to a variety of biological problems [14-16]. This method involves utilizing several hundred individual trees to reach a classification. A random sample of features/predictors is utilized for each individual tree. Here, the random forest with 128 weak learners (trees) operates with 82.02% accuracy and has an AUC of 0.8449. The best 2-Class classifier was determined to be a boosted trees ensemble utilizing RUSBoost, an algorithm which alleviates class imbalances to obtain higher accuracy [17]. The boosted trees had an overall accuracy of 82.59% accuracy and an AUC of .8841. Figure 1 shows the Receiver Operating Characteristic (ROC) curve for both the optimal 11-Class and 2-Class models.

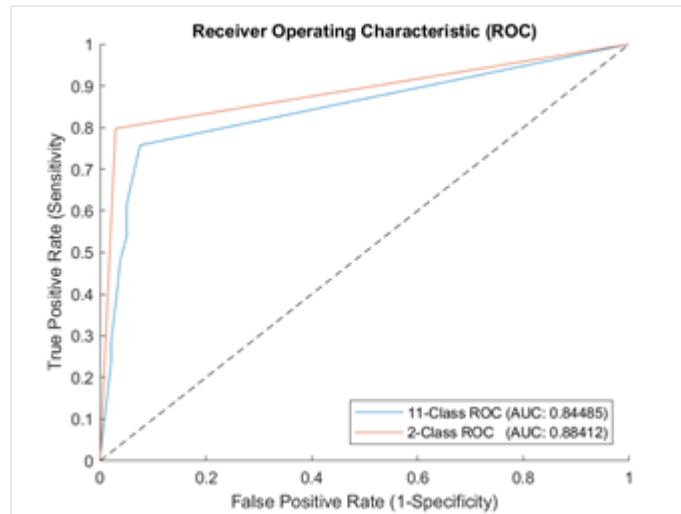


**Figure 1. Receiver Operating Characteristic (ROC) curve for both the 2-class and 11-class models, detailing the relative performances of each model.**

## 4 Discussion

The optimal model generated here, trees boosted with RUSBoost, has a specificity of 97.07%, sensitivity of 79.75%, and PPV of 94.89% when classifying heart irregularities. This shows vast improvement over both other computer models and physician-based interpretations of arrhythmia-related ECGs.

In comparison to previous machine learning projects and physician-gauged studies aimed at analyzing ECGs for cardiovascular conditions such as arrhythmia and heart failure, the algorithm presented herein had greater sensitivity, specificity, and positive predictive value (PPV). Sensitivity quantifies the ability of the proposed model to correctly detect heart irregularities amongst patients with heart irregularities. Similarly, specificity quantifies the ability of the model to detect when patients are healthy.

Compared to algorithms which utilized voting feature intervals, naive Bayes, k-nearest neighbors (KNN), support vector machines (SVM), and logistic regression, the model proposed here offers increased accuracy [6,18-20].

Additionally, both the random forest and the boosted trees offer the advantage of reduced variance given that it combines predictions from many independent weak learners. The previous studies also often utilized various cross validation methods (different training/testing splits or folds).

Furthermore, the proposed method also performed better than machine learning algorithms developed for analyzing other heart conditions, such as heart failure, with improved PPV [21]. The area under the ROC curve represents how well a classifier can distinguish between two classes (healthy or diseased).

Compared to healthcare professionals, the 2-class algorithm developed in this study had better specificity and accuracy. For instance, it outperformed cardiologists, general physicians, and general practice nurses in terms of specificity when diagnosing cardiac well-being [22]. Moreover, our false positive rate for ECG-based decision-making was 2.93%, compared to numbers as high as 41% for emergency medicine professionals when decisions needed to be made quickly [4]. Furthermore, physicians often disagree on ECG interpretations, with kappa values among cardiologists of 0.69 and among general physicians of 0.52 [3]. Kappa values indicate the rate of agreement amongst different

sources for categorical variables, and in this case, how often different doctors agreed on ECG-based diagnoses. Inaccuracies and disagreements not only delay proper treatment of patients at hand, but result in excess hospital admissions, thus delaying treatment for others. Therefore, usage of a computer algorithm for ECG-analysis would solve not only issues of accuracy, but also speed of diagnosis.

## 5 Conclusion

The best performing ensemble method proposed here functions with approximately 82.59% accuracy. Although this ensemble didn't have the highest accuracy, its sensitivity, a more transferable metric in clinical settings, was particularly high. The performance is a vast improvement over other classifiers and healthcare professionals. The highest performing ensembles tested here were the random forest and boosted trees. The ensembles, favorable to individual classifiers due to their impactful reduction on variance and improved accuracy, perform with high accuracy, sensitivity, and specificity, allowing for a proper classification of cardiological conditions in real-time.

## 6 Future Directions

More changes made in the preprocessing phase can have large impacts on the end result. Rather than removing certain patients' data and features, it may prove useful to interpolate certain datum points, collect more refined data, and investigate feature selection. Furthermore, the model developed in this experiment could be improved by introduction of further data, and a validation phase against data from outside the original data set.

## REFERENCES

- [1] Mozaffarian D, Benjamin EJ, Go AS, Arnett DK, Blaha MJ, Cushman M, et al. Heart disease and stroke statistics— 2015 update: a report from the American Heart Association. *Circulation*. 2014; 131(4):e29-322.
- [2] Drew, B., Dracup, K., Childers, R., Criley JM, Fung G, Marcus F, et al. Finding ECG Readers in Clinical Practice. *J Am Coll Cardiol*. 2014;64(5):528.
- [3] Magee C, Kazman J, Haigney M, Oriscello R, DeZee KJ, Deuster P, et al. Reliability and Validity of Clinician ECG Interpretation for Athletes. *Ann Noninvasive Electrocardiol*. 2014;19(4):319-329.
- [4] Jayes RL, Larsen GC, Beshansky JR, D'Agostino RB, Selker HP. Physician electrocardiogram reading in the emergency department—Accuracy and effect on triage decisions. *J Gen Intern Med*. 1992;7(4):387-392.
- [5] Gayathri S, Suchetha M, Latha V. ECG Arrhythmia Detection and Classification Using Relevance Vector Machine. *Procedia Eng*. 2012;38:1333-1339.
- [6] Güvenir HA, Kaçar M, Demiroz G, Cekin A. A supervised machine learning algorithm for arrhythmia analysis. *Computers in Cardiology*. 1997;24:433 - 436. 10.1109/CIC.1997.647926.
- [7] Dua D and Karra Taniskidou E. UCI Machine Learning Repository [<http://archive.ics.uci.edu/ml>]. 2017.
- [8] Mathworks. Statistics and Machine Learning Toolbox: User's Guide (r2018a). Retrieved August 01, 2018 from [https://www.mathworks.com/help/pdf\\_doc/stats/stats.pdf](https://www.mathworks.com/help/pdf_doc/stats/stats.pdf)

- [9] Schapire RE, Freund Y, Bartlett P, Lee WS. Boosting the margin: a new explanation for the effectiveness of voting methods. *The Annals of Statistics*. 1998;26(5):1651-1686.
- [10] Friedman J, Tibshirani R, Hastie T. Additive logistic regression: a statistical view of boosting (With discussion and a rejoinder by the authors). *The Annals of Statistics*. 2000;28(2):337-407.
- [11] Friedman J. Greedy Function Approximation: A Gradient Boosting Machine. Lecture presented at the: 1999; Institute of Mathematical Statistics.
- [12] Snoek J, Larochelle H, Adams RP. Practical Bayesian Optimization of Machine Learning Algorithms. arXiv:1206.2944 [stat.ML]
- [13] Breiman, L. *Machine Learning*. 2001; 45: 5.
- [14] Gray K, Aljabar P, Heckemann R, Hammers A, Rueckert D. Random forest-based similarity measures for multi-modal classification of Alzheimer's disease. *Neuroimage*. 2013;65:167-175.
- [15] Svetnik V, Liaw A, Tong C, Culberson J, Sheridan R, Feuston B. Random Forest: A Classification and Regression Tool for Compound Classification and QSAR Modeling. *J Chem Inf Comput Sci*. 2003;43(6):1947-1958.
- [16] Chen T, Cao Y, Zhang Y, Liu J, Bao Y, Wang C, et al. Random Forest in Clinical Metabolomics for Phenotypic Discrimination and Biomarker Selection. *Evidence-Based Complementary and Alternative Medicine*. 2013;2013:1-11.
- [17] Seiffert C, Khoshgoftaar TM, Van Hulse J, Napolitano A. RUSBoost: A Hybrid Approach to Alleviating Class Imbalance. *IEEE Transactions on Systems, Man, and Cybernetics - Part A: Systems and Humans*. 2010;40(1):185-197.
- [18] Zuo WM, Lu WG, Wang KQ, Zhang H. Diagnosis of cardiac arrhythmia using kernel difference weighted KNN classifier. *Computers in Cardiology*. 2008; 35:253-256.
- [19] Uyar A, Gurgen F. Arrhythmia Classification Using Serial Fusion of Support Vector Machines and Logistic Regression. 2007 4th IEEE Workshop on Intelligent Data Acquisition and Advanced Computing Systems: Technology and Applications. 2007:560-565
- [20] Soman T, Bobbie PO. Classification of Arrhythmia Using Machine Learning Techniques. *WSEAS Transactions on Computers*. 2004;4(6).
- [21] Blecker S, Katz SD, Horwitz LI, Kuperman G, Park H, Gold A, et al. Comparison of Approaches for Heart Failure Case Identification From Electronic Health Record Data. *JAMA Cardiol*. 2016;1(9):1014.
- [22] Shiyovich A, Wolak A, Yacobovich L, Grosbard A, Katz A. Accuracy of Diagnosing Atrial Flutter and Atrial Fibrillation From a Surface Electrocardiogram by Hospital Physicians: Analysis of Data From Internal Medicine Departments. *The American Journal of the Medical Sciences*. 2010;340(4):271-275.